Composite Structures 167 (2017) 262–270

Contents lists available at ScienceDirect

Composite Structures

journal homepage: www.elsevier.com/locate/compstruct

Calculation of debonding strength at the interface of particles with different shapes and matrix

E. Pérez [a,b,*], B. Lauke [c]

[a] National Scientific and Technical Research Council (CONICET), Av. Rivadavia 1917, (C1033AAJ), Buenos Aires, Argentina
[b] Plastics Research and Development Center, National Institute of Industrial Technology (INTI-Plásticos), Av. Gral. Paz 5445, (B1650KNA), San Martín, Buenos Aires, Argentina
[c] Leibniz-Institut für Polymerforschung Dresden e. V., Hohe Strasse 6, D-01069 Dresden, Germany

ARTICLE INFO

Article history:
Received 26 September 2016
Revised 16 December 2016
Accepted 3 February 2017
Available online 5 February 2017

Keywords:
Polymer-matrix composites (PMCs)
Debonding
Interface/interphase
Analytical modeling

ABSTRACT

The debonding process at the interface of filler-matrix is studied. The relevance of this process lays in its triggering effect of toughening mechanisms in polymer based composites. Based on a micromechanical model, a general approach of the debonding condition was derived. The proposed expression was applied for different particle shapes: spherical, ellipsoid, cubic, rectangular and fiber. Results of debonding strength versus geometric parameters of the different particles showed that oblate ellipsoids and cubic particles can be easily analyzed as spherical filler.

1. Introduction

Filler incorporation into polymer matrices represents a widely used technique. The aim is to obtain composite materials with enhanced mechanical performance [1–4]. On the other hand, the analysis of mechanical properties represents a really complex task due to the wide range of factors and parameters involved [1,2,5–10]. For example, particle size or content variation can promote, simultaneously, different trends for each mechanical property as: elastic modulus, stress strength, tensile toughness and fracture toughness. The relation between composite characteristics and some of these properties (e.g. elastic modulus, tensile strength) is quite well understood [1,2,11,12]. Nevertheless, theories for composite toughness are still largely discussed due to the complex tendencies experimentally observed [2,6,13,14]. Particularly, for thermoplastic composites several toughening mechanisms have been proposed: i) matrix shear yielding, ii) crazing, iii) interparticle shear yielding and iv) particle debonding followed by plastic void growth [15–18]. In general, experimental data have been analyzed by simultaneous activation of some of the listed mechanisms. Particularly, plastic void growth has been considered as a toughening mechanism extensively detected. This process is triggered by particle debonding, close related to the strength of the matrix-filler interface [14,17–21]. Based on this fact, a detailed understanding of debonding could be helpful for fracture and damage characterization.

In the present work, a general approach of the debonding stress is proposed. The general solution is applied for different particle geometries.

2. Debonding strength analysis

The simplified analyzed system consists of a particle embedded into a polymer matrix. As a first approximation, an interphase region around the particle has not been considered. In general, determination of interphase zone (mechanical properties, law of properties variation and thickness) represents a widely discussed topic. For this reason, experimental or simulated data could be incomplete, imprecise or contradictory [1,20,22–23]. Fig. 1 shows, schematically, the studied system under hydrostatic remote stress. For this loading condition, the debonding stress value could be approached by determination of the critical normal stress. In addition, stress fields around crack tips can be properly approximated by hydrostatic condition [17,20,24].

The debonding process analysis for microparticles was based on the Finite Fracture Mechanics approach considering the following conditions [20,21]:

$$\begin{aligned} -\frac{\delta U}{\delta A} &\geqslant \gamma \\ \sigma &\geqslant \sigma_{cr} \end{aligned} \tag{1}$$

* Corresponding author at: National Scientific and Technical Research Council (CONICET), Av. Rivadavia 1917, (C1033AAJ), Buenos Aires, Argentina.
E-mail address: eperez@inti.gob.ar (E. Pérez).

http://dx.doi.org/10.1016/j.compstruct.2017.02.020
0263-8223/

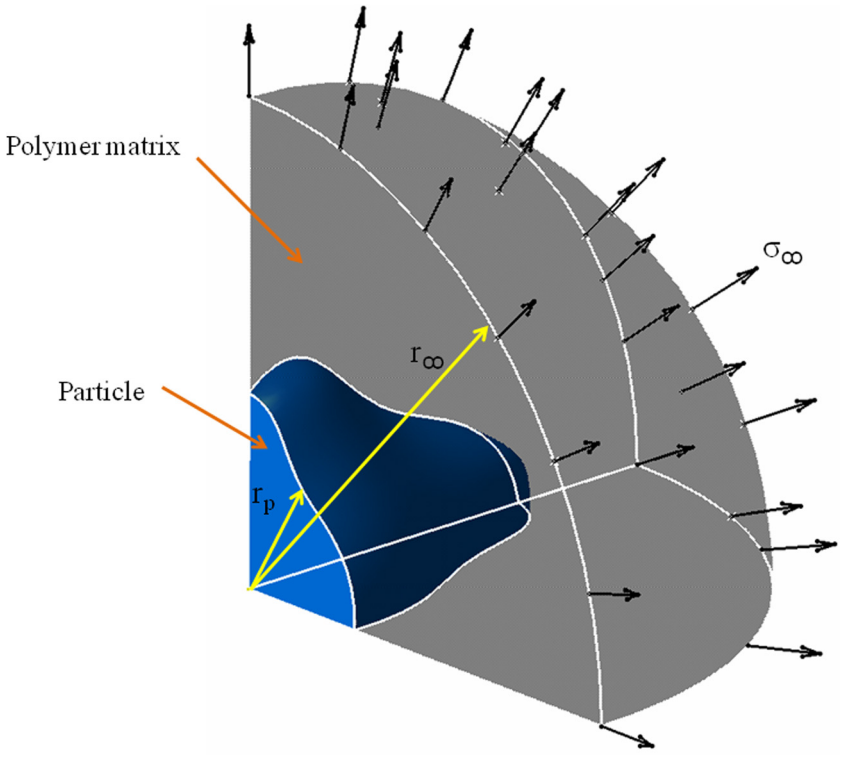

Fig. 1. Description of the analyzed system under hydrostatic remote stress.

where: γ is the interfacial fracture energy, δU is the change in potential energy of the system, σ_{cr} is the critical normal strength and δA is the debonded surface. Taking into account the equilibrium equation (before and after debonding) and neglecting the kinetic energy of the system, one obtains the energy balance equation:

$$\delta W = \delta U^m + \delta U^p + \gamma \delta A \tag{2}$$

where: δW is the work done by external forces, δU^m and δU^p are the matrix and particle elastic energy variations, respectively. The work and energy variations can be expressed as follows:

$$\delta W = \int \sigma_\infty \delta u^m_{(r_\infty)} dA^m_\infty$$

$$\delta U^p = U^p_2 - U^p_1 = 0 - \frac{1}{2}\int \sigma_{cr} u^p_1 dA^p$$

$$\delta U^m = -\frac{1}{2}\int \sigma_{cr} \delta u^m_{(r_p)} dA^m + \int \sigma_\infty \delta u^m_{(r_\infty)} dA^m_\infty$$

where: subscript 1, 2 means before and after debonding, respectively; σ_{cr} and σ_∞ are the critical and the applied stress, respectively; u^p_1 is the particle displacement value before debonding, whereas $\delta u^m_{(r_p)}$ and $\delta u^m_{(r_\infty)}$ are the matrix displacement variations at the particle surface and polymer boundary, respectively. Eq. (2) can be rewritten as follows:

$$\delta W = \int \sigma_\infty \delta u^m_{(r_\infty)} dA^m_\infty = \delta U^m + \delta U^p + \gamma \delta A$$

$$\frac{1}{2}\int \sigma_{cr} \delta u^m_{(r_p)} dA^M + \frac{1}{2}\int \sigma_{cr} u^p_1 dA^p = \gamma \delta A$$

$$\frac{1}{2}\sigma_{cr}\int [\delta u^m_{(r_p)} dA^m + u^p_1 dA^p] = \gamma \delta A$$

The new created surfaces, after debonding, are identically equal for the matrix and particle:

$$\int dA^p = \int dA^m = \int dA = \delta A$$

resulting in:

$$\frac{1}{2}\sigma_{cr}\int [\delta u^m_{(r_p)} + u^p_1] dA = \gamma \int dA$$

$$\sigma_{cr} = \frac{2\gamma \int dA}{\int [\delta u^m_{(r_p)} + u^p_1] dA}$$

while taking into account that:

$$u^m_{(r_p)} = u^m_{2(r_p)} - u^m_{1(r_p)}$$

$$\text{at}: r = r_p : u^m_{1(r_p)} = u^p_1$$

The critical stress can be rewritten as:

$$\sigma_{cr} = \frac{2\gamma \int dA}{\int u^m_{2(r_p)} dA} \tag{3}$$

The expression (3) allows some preliminary observations. The obtained equation corresponds to a general approach of the particle debonding process, independently of the filler shape, but interface continuity should be guaranteed. In addition, the critical stress value is related to the interfacial fracture energy and to the matrix displacement field, at the particle surface, after debonding.

3. Debonding stress calculation for different particle geometries

3.1. General solution for spherical particles

For a spherical symmetric problem, the general solution of the displacement field is [20,25]:

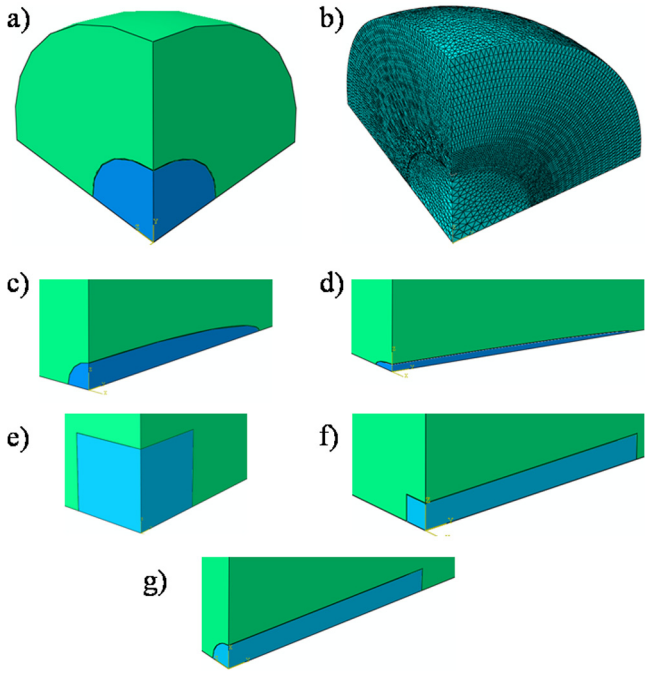

Fig. 2. Particle geometries: a) spherical, b) FE mesh, c) oblate, d) tri-axial ellipsoid, e) cubic, f) rectangular and g) fiber.

$$u = Ar + \frac{B}{r^2}$$

$$\sigma_{rr} = 3K_m A - 4G_m B\frac{1}{r^3}$$

with the following boundary conditions, after debonding:

at : $r = r_p : \sigma_{rr} = 0$

at : $r = r_\infty : \sigma_{rr} = \sigma_\infty$

where:

$$K_m = \frac{E_m}{3(1-2\nu_m)}$$

$$G_m = \frac{E_m}{2(1+\nu_m)}$$

with: E_m and ν_m as the elastic modulus and Poisson's ratio of the matrix.

The constants are expressed as the following:

$$A = \frac{\sigma_\infty}{3K_m r_p^3\left[\frac{1}{r_p^3} - \frac{1}{r_\infty^3}\right]}$$

$$B = \frac{\sigma_\infty}{4G_m\left[\frac{1}{r_p^3} - \frac{1}{r_\infty^3}\right]}$$

Thus the matrix displacement field after debonding is given by:

$$u_2^m = \frac{\sigma_\infty}{3K_m r_p^3\left[\frac{1}{r_p^3} - \frac{1}{r_\infty^3}\right]} r + \frac{\sigma_\infty}{4G_m\left[\frac{1}{r_p^3} - \frac{1}{r_\infty^3}\right]}\frac{1}{r^2}$$

$$u_2^m = \frac{\sigma_\infty}{\left[\frac{1}{r_p^3} - \frac{1}{r_\infty^3}\right]}\left[\frac{r}{3K_m r_p^3} + \frac{1}{4G_m r^2}\right]$$

where: σ_∞ can be expressed by the relation: $\sigma_{cr} = K_t\sigma_\infty$. The stress concentration factor (K_t) for uniform tension is: $K_t = 1.5$, obtained by the Finite Element Method (FEM). The critical normal strength can be calculated as:

$$\sigma_{cr} = \frac{2\gamma}{u_{2(r_p)}^m}$$

$$\sigma_{cr} = \frac{2\gamma}{\frac{\sigma_\infty}{\left[\frac{1}{r_p^3} - \frac{1}{r_\infty^3}\right]}\left[\frac{r}{3K_m r_p^3} + \frac{1}{4G_m r^2}\right]}$$

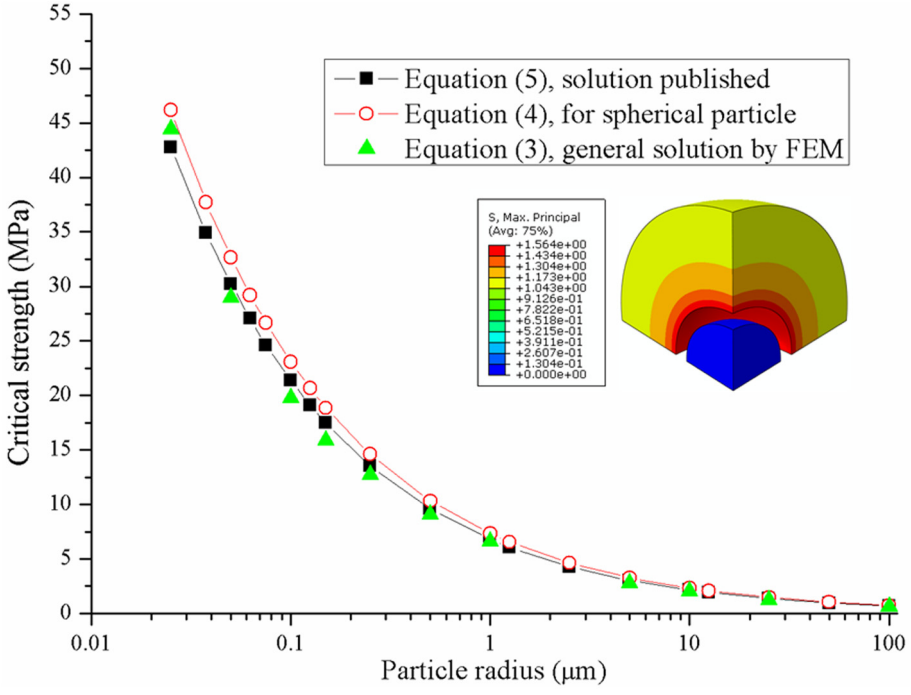

Fig. 3. Debonding stress values for spherical particles.

$$\sigma_{cr} = \frac{2\gamma}{\frac{\sigma_{cr}}{K_t\left[\frac{1}{r_p^3}-\frac{1}{r_\infty^3}\right]}\left[\frac{r}{3K_m r_p^3}+\frac{1}{4G_m r^2}\right]}$$

Resulting in:

$$\sigma_{cr}^2 = \frac{2\gamma}{\frac{1}{K_t\left[\frac{1}{r_p^3}-\frac{1}{r_\infty^3}\right]}\left[\frac{r}{3K_m r_p^3}+\frac{1}{4G_m r^2}\right]}$$

$$\sigma_{cr}^2 = \frac{2\gamma K_t\left[\frac{1}{r_p^3}-\frac{1}{r_\infty^3}\right]}{\left[\frac{r}{3K_m r_p^3}+\frac{1}{4G_m r^2}\right]}$$

Since: $r_\infty \gg r_p$, the equation can be rewritten as:

$$\sigma_{cr}^2 = \frac{\frac{2\gamma K_t}{r_p^3}}{\left[\frac{r}{3K_m r_p^3}+\frac{1}{4G_m r^2}\right]}$$

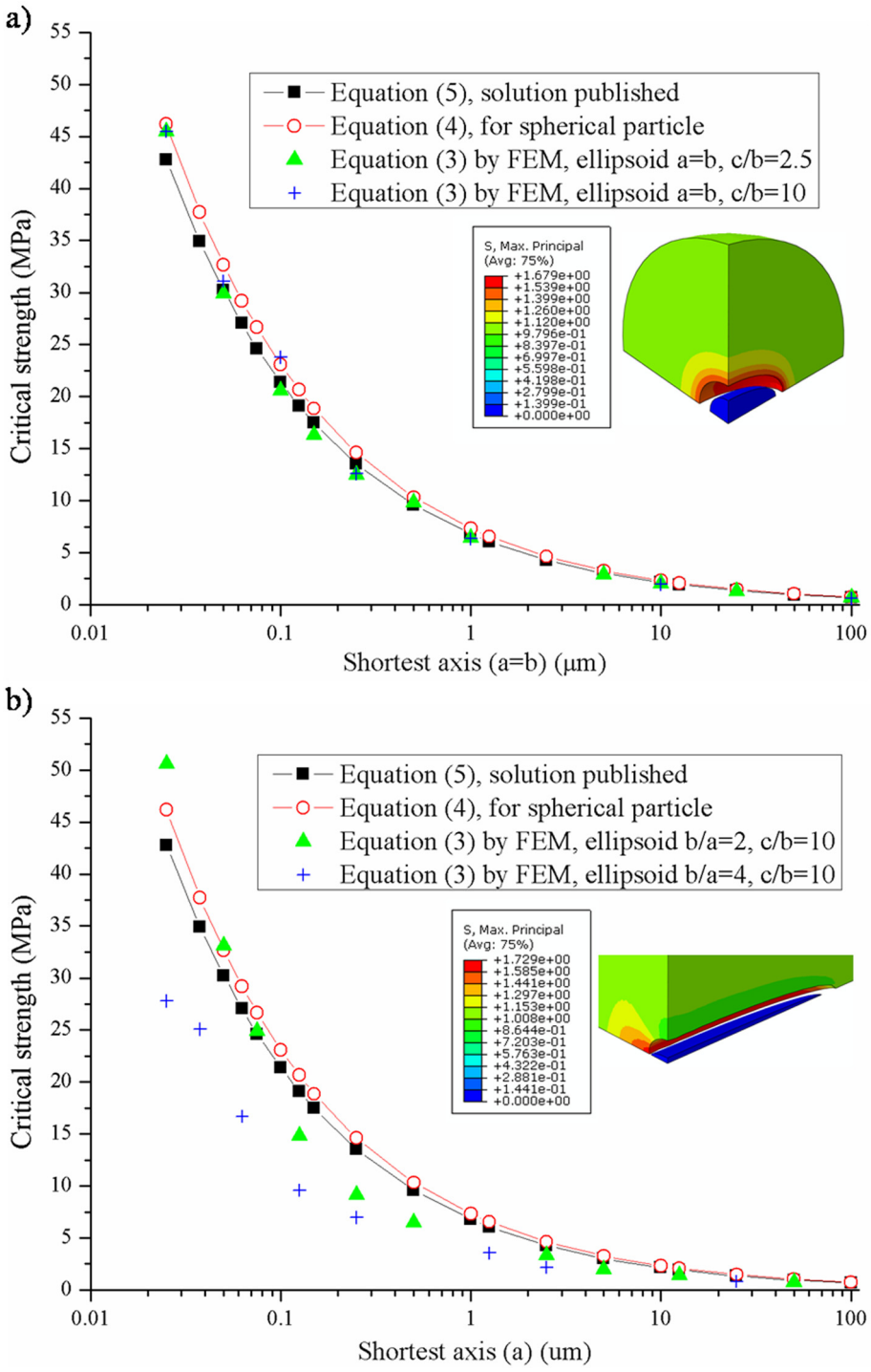

Fig. 4. Debonding stress values for: a) oblates and b) tri-axial ellipsoids.

For $r = r_p$ this relation leads to:

$$\sigma_{cr}^2 = \frac{\frac{2\gamma K_t}{r_p^3}}{\left[\frac{1}{3K_m r_p^2} + \frac{1}{4G_m r_p^2}\right]}$$

$$\sigma_{cr}^2 = \frac{\frac{2\gamma K_t}{r_p^3}}{\left[\frac{4G_m + 3K_m}{12G_m K_m r_p^2}\right]}$$

$$\sigma_{cr}^2 = \frac{2\gamma K_t}{r_p^3} \frac{12G_m K_m r_p^2}{(4G_m + 3K_m)}$$

$$\sigma_{cr}^2 = \frac{2\gamma K_t}{r_p} \frac{12G_m K_m}{(4G_m + 3K_m)}$$

And this finally provides:

$$\sigma_{cr} = \sqrt{\frac{24\gamma K_t}{r_p} \frac{G_m K_m}{(4G_m + 3K_m)}}$$

which can be simplified into the expression:

$$\sigma_{cr} = \sqrt{\frac{4}{3} \frac{\gamma E_m K_t}{(1 - \nu_m)} \frac{1}{r_p}} \tag{4}$$

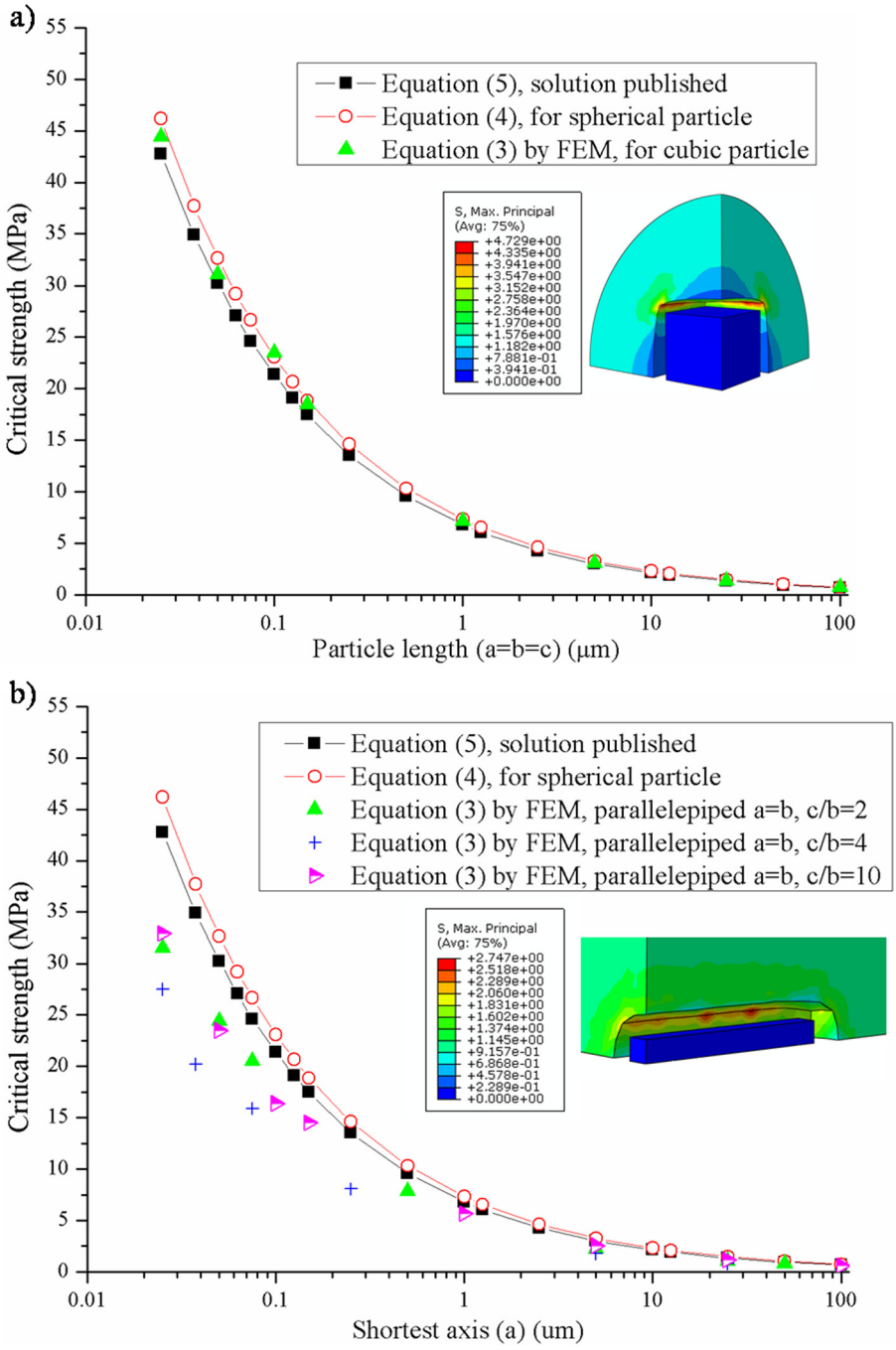

Fig. 5. Debonding stress values for: a) cubic and b) rectangular particles.

3.2. Debonding stress calculation for spherical particles

Similar analytical solutions for spherical particle have been published by other authors [17,20,21]:

$$\sigma_{cr} \cong \sqrt{\frac{4\gamma}{r_p}\frac{E_m}{(1+\upsilon_m)}} \tag{5}$$

The general solution (Eq. (3)) and the particular solution for spherical inclusion (Eq. (4)) were compared with the published expression (Eq. (5)), in order to verify the accuracy of the proposed model. The following parameter values were considered:

- matrix: $\gamma = 0.01$ J/m^2; $E_m = 1.6$ GPa; $\upsilon_m = 0.4$
- particle: $E_p = 16$ GPa; $\upsilon_p = 0.2$

The displacement values required for the general solution (Eq. (3)) were obtained by FEM. The modeled system consists of an axisymmetrical problem: a spherical particle (Fig. 2.a) within a polymer region under tension applied at the boundary. Linear elastic material behaviors were adopted for the spherical particle and polymer matrix. The mesh (Fig. 2.b) was built by 10-node elements and refined in the interphase between components. All calculations were performed by ABAQUS 6.13-4 and the stress distribution is plotted in Fig. 3. The critical strength values (Fig. 3) obtained with the different expressions exhibited similar tendencies with particle radius variation.

3.3. General solution for elliptical particles

The general solution (Eq. (3)) was considered now for elliptical particles with the geometries shown in Fig. 2.c and .d and the required displacement values were obtained by FEM. In addition, models for different particle shapes (ellipsoidal, cubic, rectangular, fiber) were developed similarly to previous described for spherical situation. For the analysis of ellipsoids different semi-axis relations and particle cross section were considered:

- a = b, c/b = 2.5 (circular cross section, oblate).
- a = b, c/b = 10 (circular cross section, oblate).
- b/a = 2, c/b = 10 (elliptical cross section, tri-axial ellipsoid).
- b/a = 4, c/b = 10 (elliptical cross section, tri-axial ellipsoid).

The critical stress values were plotted as a function of the shortest semi-axis. Fig. 4 shows the obtained results for ellipsoids with circular and elliptical cross section. For circular cross section (Fig. 4.a), the corresponding critical stress values were similar to the spherical particles. These geometries could be easily analyzed as a spherical situation by Eqs. (4) or (5). On the other hand, particles with elliptical cross section (Fig. 4.b) displayed some discrepancies. Ellipsoids with the largest semi-axis relations (b/a = 4 and c/b = 10) showed reduced critical stress values at short particle sizes.

3.4. General solution for cubic particles

For cubic particle (Fig. 2.e), the general solution (Eq. (3)) was considered. The displacement values required were obtained by FEM, in a similar way as previously described. The obtained results for cubic filler (Fig. 5.a) were similar to the spherical solutions, independently of the filler size.

3.5. General solution for rectangular particles

For this geometry (Fig. 2.f) different semi-axis relations were considered:

- a = b, c/b = 2, (square cross section).
- a = b, c/b = 4, (square cross section).
- a = b, c/b = 10, (square cross section).

Fig. 5.b shows the obtained results for rectangular particles; shortest semi-axis variations were plotted. For filler sizes shorter than 1 μm, the corresponding critical stress values were lower than the spherical solutions.

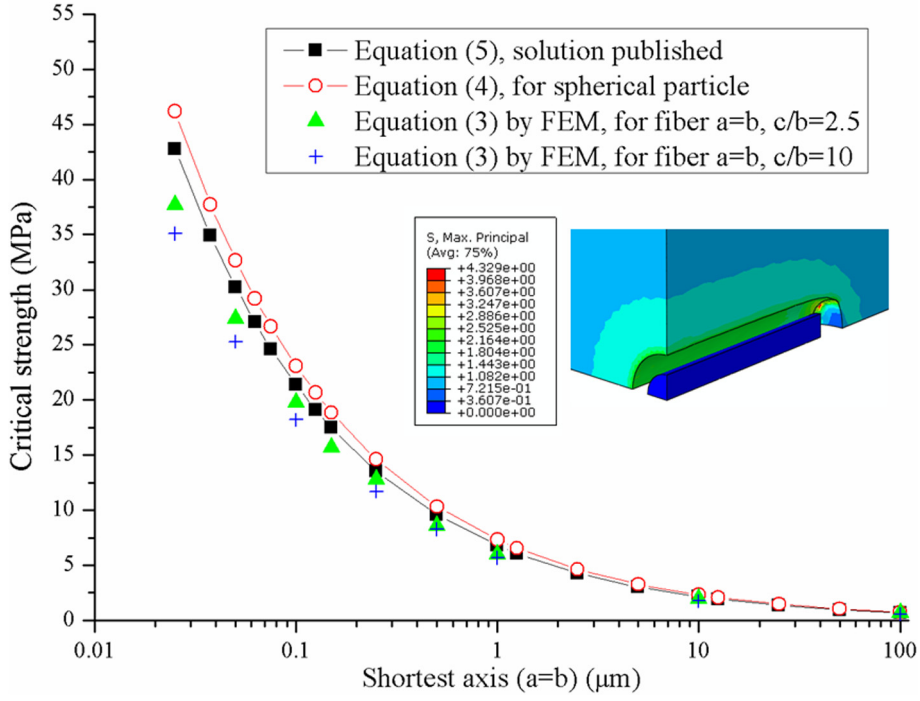

Fig. 6. Debonding stress values for fibers.

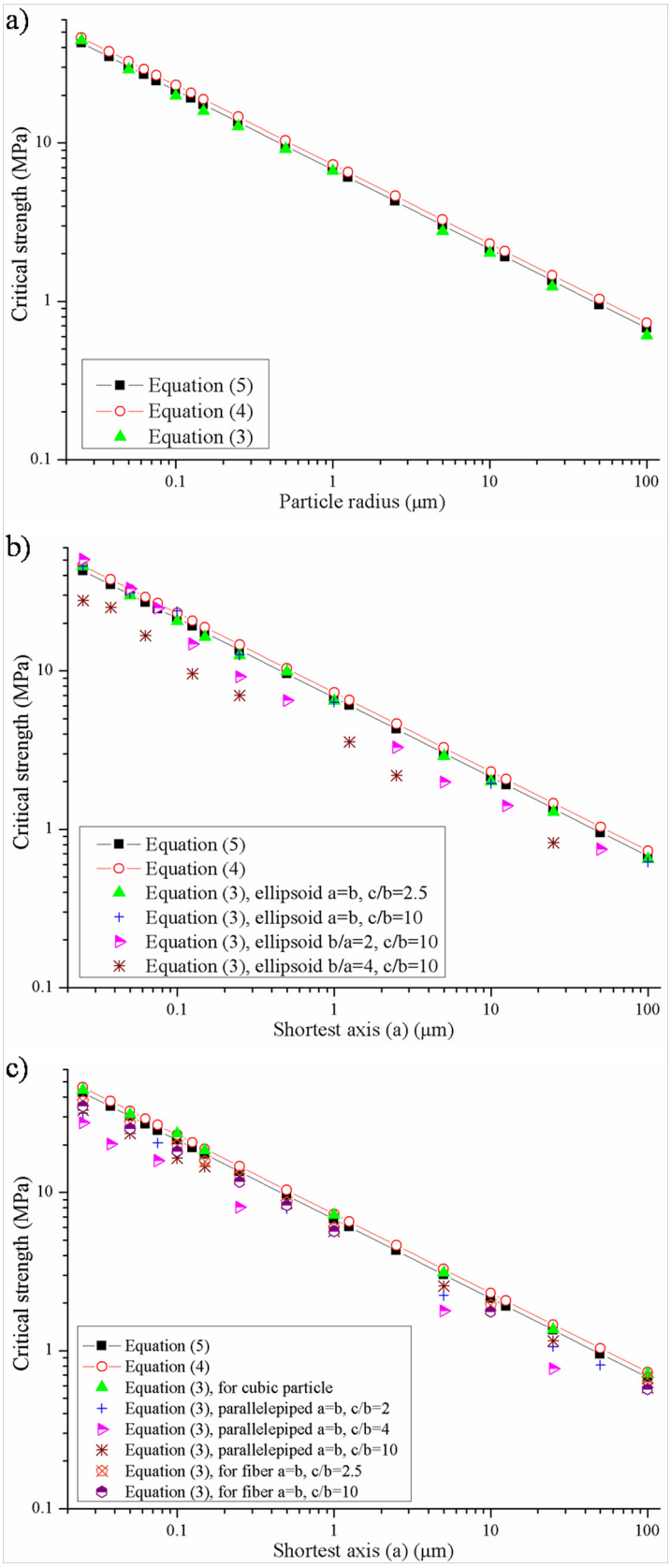

Fig. 7. Critical strength values for: a) spherical particles, b) ellipsoids and c) cubic, rectangular particles and fiber.

Table 1
Slopes for the different particle shapes.

	Slope	r^2
Spherical particle		
Eq. (3)	−0.51	0.999
Eq. (4)	−0.50	0.999
Eq. (5)	−0.50	0.999
Ellipsoids		
a = b, c/b = 2.5	−0.51	0.999
a = b, c/b = 10	−0.52	0.998
b/a = 2, c/b = 10	−0.55	0.989
b/a = 4, c/b = 10	−0.52	0.989
Cubic particle		
a = b = c	−0.50	0.999
Parallelepiped		
a = b, c/b = 2	−0.49	0.998
a = b, c/b = 4	−0.51	0.999
a = b, c/b = 10	−0.48	0.999
Fiber		
a = b, c/b = 2.5	−0.49	0.999
a = b, c/b = 10	−0.50	0.999

3.6. General solution for fibers

The fiber geometry is shown in Fig. 2.g and the semi-axis relations considered were:

- a = b, c/b = 2.5 (circular cross section).
- a = b, c/b = 10 (circular cross section).

Fibers (Fig. 6) shorter than 1 μm exhibited slightly lower values than the spherical solutions.

Based on the obtained results previously described, some observations can be introduced. Reduced critical stress values were observed for inclusions with no symmetric stress distributions (e.g. tri-axial ellipsoids) compared with the spherical solution. The no axisymmetrically stress distributions around particle surface could easily trigger the debonding process, but this observation should be extensively analyzed.

Fig. 7 shows the critical strength for the different particle geometries analyzed. Debonding process, related to the particle size, can be promoted by the interface fracture toughness or by the interfacial strength [26]. In the region where debonding process depends on interface fracture toughness, a characteristic slope can be determined. In general, for the analyzed particles (Table 1) the slopes were close to 0.5, similar to previously reported ones for fibers [26]. In addition, tri-axial ellipsoids and rectangular particles exhibited increased values.

3.7. Experimental data compared to general solution for elliptical particles

The tensile strength of composite materials has been related to the debonding process [1,2]. Large filler sizes, agglomerates and weak interface strength can promote a reduction of this parameter. In a previous work, quartz distribution into a polypropylene (PP) matrix and filler-matrix interaction were investigated. Relatively weak interface strength was estimated. Particle size distributions were irregular and broader with increased filler content [10]. In addition, quartz particles ($E_p = 72$ GPa; $\nu_p = 0.17$) exhibited morphologies similar to ellipsoids (semi-axis relation: c/b = 2, approximately). Debonding stress was determined based on results of Section 3.3 and median particle size for each PP-quartz composite. Fig. 8 shows similar trends for experimental and theoretical analysis (tensile strength of PP-quartz composites and critical debonding stress) but with a large difference on their values. It should be remarked that the debonding process affects the composite tensile strength but does not limit it. In addition, proposed debonding solution does not consider matrix yielding or plastic void growth. Finally, in order to obtain a deeper understanding of

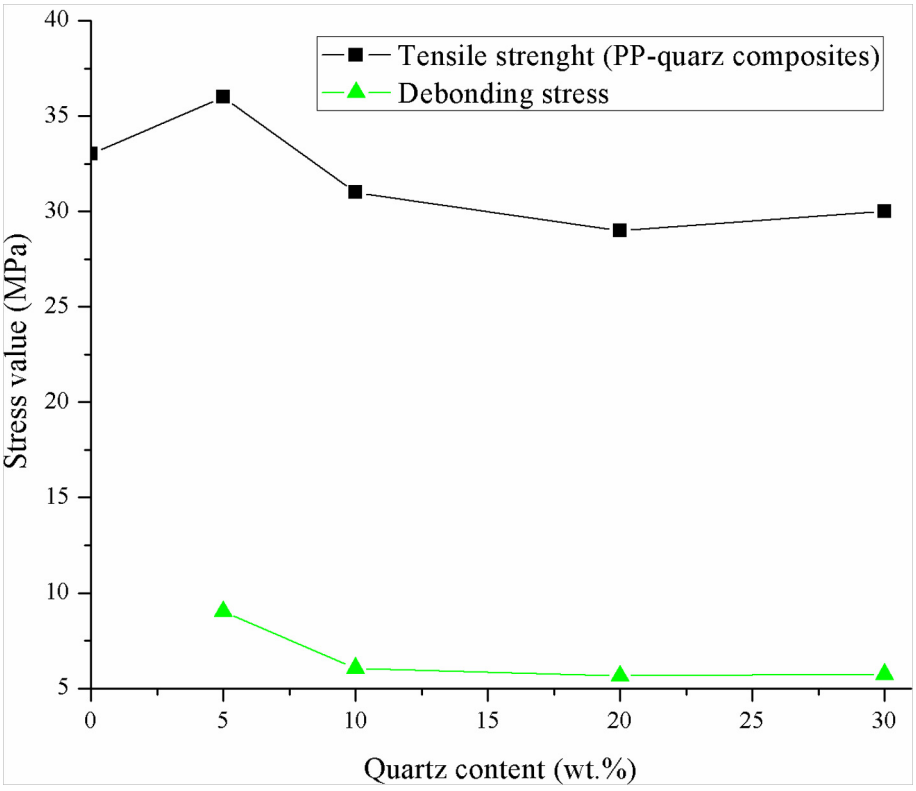

Fig. 8. Debonding stress values and tensile strength of PP-quartz composites.

polymer composite mechanical behavior, several authors highlight the importance to develop multi-scale modeling strategies and their experimental validation [27,28]. In particular, for debonding stress, published experimental data suggest that the process depends on particle size but, unfortunately, it has not been proved yet.

4. Conclusions

In this work, a general approach to determine the particle debonding stress was proposed. The analysis performed was based on a micromechanical model meaning that the solution should be restricted to this scale, due to none nanoscale effects have been taken into account. The general expression was applied for different particle shapes. Comparison with spherical expressions, previously published, allows validating the solution proposed.

Obtained results suggest that some particle geometries with semi-axis relation: $a = b$ (oblate ellipsoids and cubic particles) can be easily analyzed as spherical filler. On the other hand, in all cases the highest discrepancies were observed for short filler sizes (lower than 1 μm).

Acknowledgement

The authors want to acknowledge to the German Academic Exchange Service (DAAD) and to the National Research Council of Argentina (CONICET) for the financial support.

References

[1] Móczó J, Pukánszky B. Polymer micro and nanocomposites: structure, interactions, properties. J Ind Eng Chem 2008;14:535–63.
[2] Fu SY, Feng XQ, Lauke B, Mai YW. Effects of particle size, particle/matrix interface adhesion and particle loading on mechanical properties of particulate–polymer composites. Comp: B 2008;39:933–61.
[3] Mukhopadhyay S, Deopura BL, Alagiruswamy R. Interface behavior in polypropylene composites. J Thermo Comp Mat 2003;16:479–95.
[4] Pukánszky B. Interfaces and interphases in multi component materials: past, present, future. Eur Pol J 2005;41:645–62.
[5] Avella M, Cosco S, Di Lorenzo ML, Di Pace E, Errico ME, Gentile G. Nucleation activity of nanosized $CaCO_3$ on crystallization of isotactic polypropylene, in dependence on crystal modification, particle shape, and coating. Eur Pol J 2006;42:1548–57.
[6] Liu ZH, Kwok KW, Li RKY, Choy CL. Effects of coupling agent and morphology on the impact strength of high density polyethylene/$CaCO_3$ composites. Pol 2002;43:2501–6.
[7] Lertwimolnun W, Vergnes B. Influence of compatibilizer and processing conditions on the dispersion of nanoclay in a polypropylene matrix. Pol 2005;46:3462–71.
[8] Zhang YH, Bai BF, Li JQ, Chen JB, Shen CY. Multifractal analysis of the tensile fracture morphology of polyvinylidenechloride/glass fiber composite. Appl Surf Sci 2011;257:2984–9.
[9] Diéz-Gutiérrez S, Rodríguez-Pérez MA, De Saja JA, Velasco JI. Dynamic mechanical analysis of injection-moulded discs of polypropylene and untreated talc filled polypropylene composites. Pol 1999;40:5345–53.
[10] Pérez E, Bernal C, Pérez CJ. Internal structure analysis of polypropylene/quartz composites related to their toughness. Pol Comp 2016;37:1488–96.
[11] Verbeek CJR. The influence of interfacial adhesion, particle size and size distribution on the predicted mechanical properties of particulate thermoplastic composites. Mat Lett 2003;57:1919–24.
[12] Kiss A, Fekete E, Pukánszky B. Aggregation of $CaCO_3$ particles in PP composites: effect of surface coating. Comp Sci Technol 2007;67:1574–83.
[13] Cotterell B, Chia JYH, Hbaieb K. Fracture mechanisms and fracture toughness in semicrystalline polymer nanocomposite. Eng Fract Mech 2007;74:1054–78.
[14] Lauke B. On the effect of particle size on fracture toughness of polymer composites. Comp Sci Technol 2008;68:3365–72.
[15] Deblieck RAC, van Beek DJM, Remerie K, Ward IM. Failure mechanisms in polyolefines: the role of crazing, shear yielding and the entanglement network. Pol 2011;52:2979–90.
[16] Zuiderduin WCJ, Westzaan C, Huétink J, Gaymans RJ. Toughening of polypropylene with calcium carbonate particles. Pol 2003;44:261–75.
[17] Williams JG. Particle toughening of polymers by plastic void growth. Comp Sci Technol 2010;70:885–91.
[18] Thio YS, Argon AS, Cohen RE. Role of interfacial adhesion strength on toughening polypropylene with rigid particles. Pol 2004;45:3139–47.
[19] Karger-Kocsis J, Khumalo VM, Bárány T, Mészáros L, Pegoretti A. On the toughness of thermoplastic polymer nanocomposites as assessed by the essential work of fracture (EWF) approach. Comp Inter 2013;20(6):395–404.
[20] Zappalorto M, Salviato M, Quaresimin M. Influence of the interphase zone on the nanoparticle debonding stress. Comp Sci Technol 2011;72:49–55.
[21] Chen JK, Huang ZP, Zhu J. Size effect on the damage dissipation in nanocomposites. Comp Sci Technol 2007;67:2990–6.
[22] Vörös G, Pukánszky B. Effect of a soft interlayer with changing properties on the stress distribution around inclusions and yielding of composites. Comp: A 2001;32:343–52.
[23] Quaresimin M, Salviato M, Zappalorto M. A multi-scale and multi-mechanism approach for the fracture toughness assessment of polymer nanocomposites. Comp Sci Technol 2014;91:16–21.
[24] Chen JK, Huang ZP, Mai YW. A constitutive relation of particulate-reinforced viscoelastic composite materials with debonded microvoids. Acta Mater 2003;51:3375–84.
[25] Lauke B, Schüller T, Beckert W. Calculation of adhesion strength at the interface of a coated particle embedded within matrix under multiaxial load. Comp Mat Sc 2000;18:362–80.
[26] Carraro PA, Zappalorto M, Quaresimin M. A comprehensive description of interfibre failure in fibre reinforced composites. Theor Appl Fract Mech 2015;79:91–7.
[27] Dastgerdi JN, Marquis G, Salimi M. Micromechanical modeling of nanocomposites considering debonding of reinforcements. Comp Sci Technol 2014;93:38–45.
[28] Quaresimin M, Salviato M, Zappalorto M. Strategies for the assessment of nanocomposite mechanical properties. Comp: B 2012;43:2290–7.